International Journal of Minerals, Metallurgy and Materials
Volume 26, Number 2, February 2019, Page 241
https://doi.org/10.1007/s12613-019-1729-5

Effect of pre-recovery on microstructure and properties of rolled Al–12.18Zn–3.31Mg–1.43Cu–0.20Zr–0.04Sr aluminum alloy

Cheng-bin Cai, Xiao-jing Xu, Jin-dong Huang, Shi-hao Ju, Qing Ding, and Cheng-song Wang

Engineering Institute of Advanced Manufacturing and Modern Equipment Technology, Jiangsu University, Zhenjiang 212013, China
(Received: 25 April 2018; revised: 25 October 2018; accepted: 30 October 2018)

Abstract: The independently designed and manufactured ultra-high-strength aluminum alloy Al–12.18Zn–3.31Mg–1.43Cu–0.20Zr–0.04Sr was investigated via scanning electron microscopy observations, X-ray diffraction analysis, hardness tests, electrical conductivity tests, tensile tests, intergranular corrosion tests, and exfoliation corrosion tests. The effect of pre-recovery on the microstructure and mechanical properties of this aluminum alloy was also studied. The results show that the pre-recovery heat treatment releases deformation energy, inhibits recrystallization, and decreases the dislocation density. Although the pre-recovery heat treatment has little effect on the hardness, electrical conductivity, and elongation of this aluminum alloy, it can dramatically improve the alloy's tensile strength (the maximum tensile strength increased from 785.0 MPa to 809.2 MPa). Moreover, the tensile properties of this aluminum alloy have a certain degree of isotropy, and the pre-recovery heat treatment does not affect this property. In addition, the rolled aluminum alloy exhibits good corrosion resistance, but the effect of the pre-recovery heat treatment on the alloy's resistance to intergranular and exfoliation corrosion is negligible.

Keywords: ultra-high strength aluminum alloy; pre-recovery; microstructure; mechanical property; corrosion resistance

1. Introduction

Since the twentieth century, ultra-high-strength aluminum alloy has been widely used in the aerospace, automobile, shipping, and defense industries because of its advantages of low density, high specific strength, high corrosion resistance, and good machinability [1–3]. With the development of modern industry, the manufacturing industry has placed additional requirements on the performance of super-strength aluminum alloy. Therefore, the use of existing technology to further optimize the microstructure and overall performance of aluminum alloys is currently an active research topic.

Ultra-high-strength aluminum alloy, after rolling processing, contains numerous defects such as dislocations and texture. In addition, rolling can produce a large amount of deformation energy, which is prone to recrystallization in subsequent heat treatment processes and severely weakens the alloy's comprehensive performance [4–6]. For example, if hot extruded aluminum alloy is recrystallized, the deformation strengthening structure (such as the extruded structure) will be weakened and the deformation strengthening effect of the alloy will be diminished. Xu *et al.* [7] found that pre-recovery heat treatment can substantially refine the grain size, inhibit recrystallization, and enhance the material's strength. Sun *et al.* [8] studied the impact of pre-recovery on the microstructure and properties of Al–Zn–Mg–Cu super-strength aluminum alloy in the T652 state; their results showed that pre-recovery can reduce the alloy's dislocation density and improve its resistance to intergranular corrosion and exfoliation corrosion.

Thus far, the effect of pre-recovery heat treatment on the microstructure and properties of rolled ultra-high-strength aluminum alloy has rarely been studied, and the mechanism of the pre-recovery heat treatment is not clear. Therefore, the effect of pre-recovery on the microstructure and properties of rolled ultra-high-strength aluminum alloy is an important research topic. In this paper, the effect of pre-recovery heat treatment on the microstructure and properties of Al–12.18Zn–3.31Mg–1.43Cu–0.20Zr–0.04Sr aluminum

Corresponding author: Xiao-jing Xu E-mail: xjxu67@126.com

alloy was studied to provide reference data for further performance optimization.

2. Experimental

The raw materials for casting the aluminum alloy were industrial pure Al (99.79wt% Al), Zn (99.9wt% Zn), Mg (99.9wt% Mg), Al–Cu master alloy with 50.12wt% Cu, Al–Zr master alloy with 4.11wt% Zr, and Al–Sr master alloy with 9.89wt% Sr. On the basis of our previous experimental experience, to obtain high strength, the Zn and Mg contents were designed to be ~12.1wt% and ~3.3wt%, respectively. At the same time, to balance the corrosion resistance, the content of Cu was designed to be ~1.4wt%. In addition, a small amount of Zr and Sr was also added. The measured composition of the aluminum alloy was Al–12.18Zn–3.31Mg–1.43Cu–0.20Zr–0.04Sr. After melting and casting, the ingot was subjected to a homogenization heat treatment: First, the ingot was insulated for a certain period and the heat preservation process was 400°C × 6 h + 420°C × 6 h + 440°C × 6 h + 460°C × 12 h. The material was then removed from the furnace, cooled to room temperature in air, and subjected to extrusion processing with an extrusion ratio of 12. The rolled samples were cut from the extruded bar, and the samples were rolled seven passes in total. The first four passes were rolled with a reduction of 2 mm with each pass; the subsequent three passes were rolled with a reduction of 1.5 mm. The rolling direction of the sample was unchanged during the whole process, and the sample was finally rolled into a 4-mm-thick sheet.

The experimental samples were divided into two groups; the first group was used for comparison. The processing technology for the first group was rolling–solution-aging; that for the second group was rolling–pre-recovery–solution-aging. The pre-recovery processing was 250°C × 24 h + 300°C × 6 h + 350°C × 6 h + 400°C × 6 h, the solution processing was 450°C × 2 h + 460°C × 2 h + 470°C × 2 h, and the aging processing were T6 (121°C × 24 h), T7X-1 (121°C × 5 h + 153°C × 16 h) and T7X-2 (121°C × 5 h + 133°C × 16 h). After solution treatment, the samples were removed from the furnace and then immediately subjected to water quenching. After the heat treatment was completed, the tensile and metallographic specimens were prepared as shown in Fig. 1; the size of the tensile test sample is shown in Fig. 2.

The microstructure of the alloy was observed using a JSM-IT300 scanning electron microscope equipped with an energy-dispersive spectromete. The XRD analysis was performed on a D8 Advance X-ray diffractometer manufactured by Bruker. Cu radiation at a wavelength of 0.15406 nm

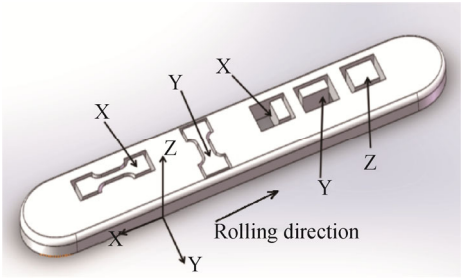

Fig. 1. Sampling physical map of the rolling sample.

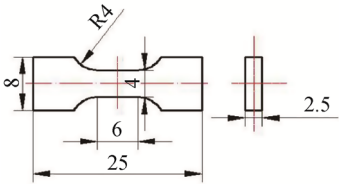

Fig. 2. Dimensions of the tensile sample (unit: mm).

was used in the XRD analysis. The scanning range was from 30° to 120° and the scanning speed was 5°/min. The hardness of the material was measured with a HV-1000 hardness tester. The conductivity of the material was measured with a model 7501 eddy current conductivity meter, and the conductivity tests were performed according to standard GB/T 12966–2008. The tensile properties were tested using a domestic WDW-200 tensile machine, and the resistance to intergranular corrosion and exfoliation corrosion of this alloy was tested in accordance with standards GB 7998–2005 and GB/T 22639–2008, respectively. In accordance with standard GB 7998–2005, the samples were first placed in 10wt% NaOH solution for 10 min, then placed in 30wt% HNO_3 solution for 3 min, and finally placed in a corrosive solution (57 g/L NaCl + 10 mL/L H_2O_2 + H_2O) and kept at 35°C for 6 h. The intergranular corrosion depth was then measured using an optical microscope. In accordance with standard GB/T 22639–2008, the samples were placed into an exfoliation corrosive solution (4.0 mol/L NaCl + 0.5 mol/L KNO_3 + 0.1 mol/L HNO_3 + H_2O) at 25°C for 48 h. The samples were then removed and placed into concentrated HNO_3 for 30 s, and the exfoliation corrosion morphologies were observed. In addition, a 4XC-MS optical microscope was used to observe the microstructure and intergranular corrosion depth of the alloy.

3. Results and discussion

3.1. Microstructure

Fig. 3 shows the microstructure of Al–12.18Zn–3.31Mg–1.43Cu–0.20Zr–0.04Sr aluminum alloy subjected to different heat treatment processes, as observed in the *Z* direction.

The results in Fig. 3 show that the grain size of the alloy after the rolling process was very small and that the majority of the grains were smaller than 5 μm. The grain size of the rolled aluminum alloy after the heat treatment process increased substantially. Figs. 3(b) and 3(c) shows that the grain size of the alloy after the rolling–pre-recovery–solution treatment increased slightly compared with that after rolling–solution treatment. The increase of the grain size can consume part of the deformation energy and reduce the recrystallization driving force [9–11]. It can also inhibit recrystallization and improve the corrosion resistance. In addition, after rolling processing, a large number of black areas were observed in the alloy, some of which are undissolved second phase. The amount of undissolved second phase was substantially reduced when the alloy was subjected to solution or pre-recovery–solution treatment; however, because of the high degree of alloying, the residual second phase could not be completely eliminated. By comparison, after rolling–solution treatment, numerous gray areas were observed near the grain boundaries; most of these areas are undissolved second phase. Nevertheless, the gray area was obviously reduced when the aluminum alloy was subjected to rolling–pre-recovery–solution heat treatment. This phenomenon indicates that the pre-recovery heat treatment can further promote the dissolution of the undissolved second phase.

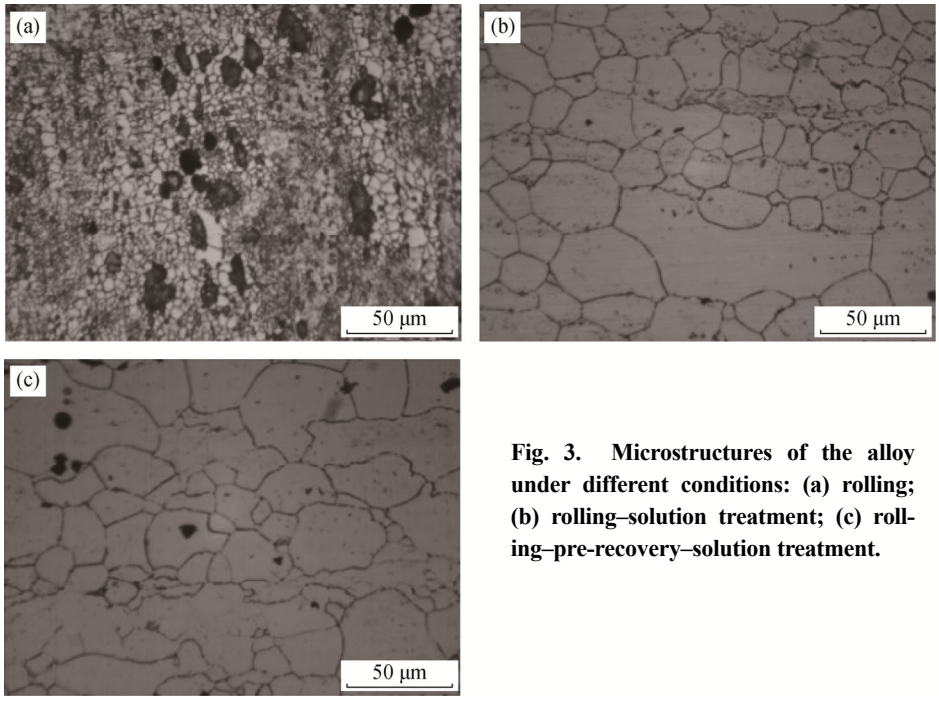

Fig. 3. Microstructures of the alloy under different conditions: (a) rolling; (b) rolling–solution treatment; (c) rolling–pre-recovery–solution treatment.

To further explore the specific composition of the undissolved second phase in the alloy, energy-dispersive spectroscopy (EDS) was performed on the regions shown in Fig. 4, where the A, C, and E regions are the matrix and the remaining regions are the undissolved second phase. The analysis results are listed in Table 1. The results of the EDS analysis show that the matrix composition differs slightly when the alloy is subjected to different processes. Compared with the Zn and Mg contents in the matrix of the alloy without heat treatment, those in the matrix of the alloy after solution and pre-recovery–solution heat treatment were increased; however, the Cu content was slightly decreased. Compared with the Zn, Mg, and Cu contents of the matrix, those of areas B, D, F, and H are substantially greater.

3.2. XRD analysis and dislocation density

The XRD pattern of pure aluminum is shown in Fig. 5, and the XRD patterns and full-widths at half-maxima (FWHMs) of the peaks of Al–12.18Zn–3.31Mg–1.43Cu–0.20Zr–0.04Sr aluminum alloy samples subjected to different heat treatment processes are shown in Fig. 6. Comparing Fig. 5 with Fig. 6 reveals that, after the heat treatment, the position and intensity of the diffraction peaks of the alloy changed to a great extent, which indicates that the heat treatment substantially changed the alloy's crystal orientation. A comparison of Figs. 6(b) and 6(d) shows that the diffraction peak position and intensity of the alloy are almost unchanged, illustrating that the pre-recovery heat treatment had little effect on the crystal orientation of this aluminum alloy.

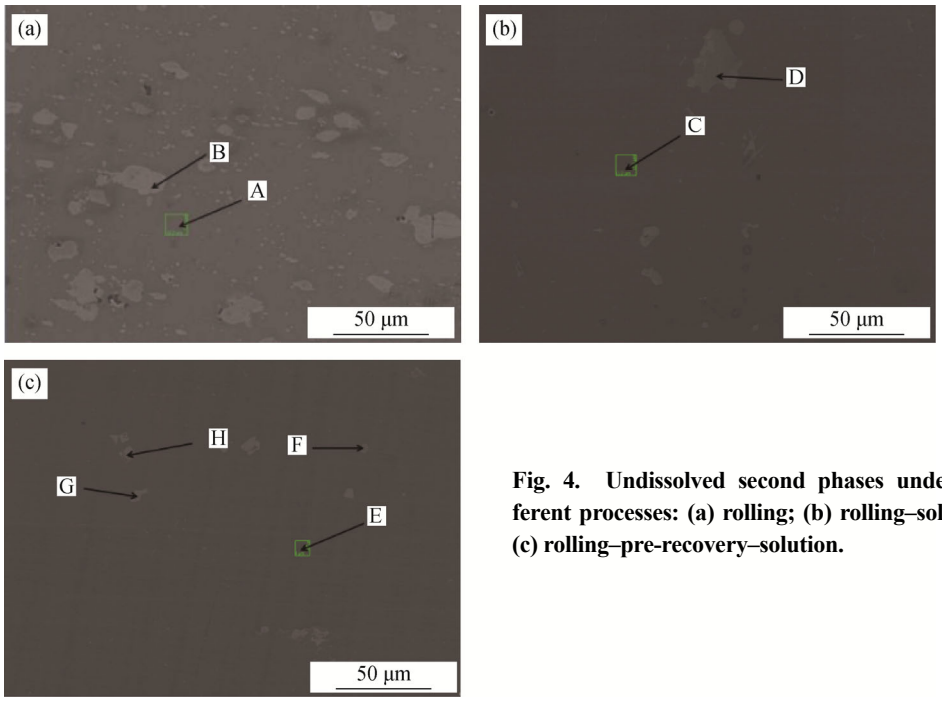

Fig. 4. Undissolved second phases under different processes: (a) rolling; (b) rolling–solution; (c) rolling–pre-recovery–solution.

Table 1. The composition of the undissolved second phase wt%

Region	Al	Zn	Mg	Cu	Sr	Zr
A	87.34	8.70	2.79	1.01	0.07	0.09
B	19.03	52.28	21.02	7.35	0.25	0.07
C	85.48	9.89	3.58	0.67	0.33	0.05
D	35.31	41.10	15.00	8.20	0.29	0.09
E	84.83	10.17	3.73	0.91	0.23	0.13
F	57.42	26.93	8.57	6.48	0.48	0.11
G	38.41	29.45	1.64	16.40	12.54	1.57
H	37.62	40.77	14.49	6.77	0.27	0.07

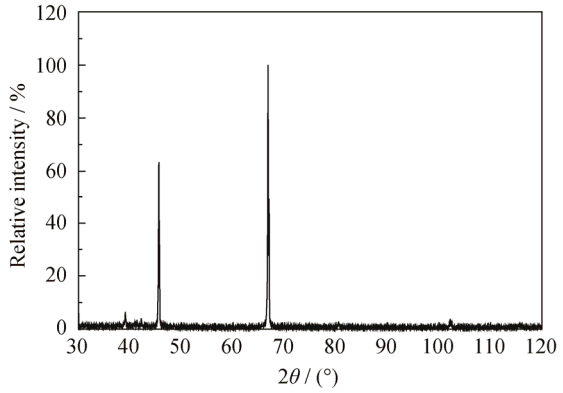

Fig. 5. The XRD pattern of pure Al powder.

The dislocation density can be calculated from XRD data, and the relationship among the dislocation density (ρ), size of the XRD coherent diffraction zone (d), and the lattice strain (e) is described by the following function [12]:

$$\rho = 2\sqrt{3}\langle e^2\rangle^{1/2}/db \quad (1)$$

In this function, b represents the Burgers vector (for Al, b = 0.286 nm).

The relationship among (d), (e), the half-height peak width ($\delta 2\theta$), the peak position of each diffraction peak (θ_0), and the wavelength of Cu K_α radiation (λ) is described by the following function [13]:

$$\frac{(\delta 2\theta)^2}{\tan^2\theta_0} = 25\langle e\rangle^2 + \frac{\lambda}{d}\left(\frac{\delta 2\theta}{\tan\theta_0 \sin\theta_0}\right) \quad (2)$$

The relationship between $(\delta 2\theta)^2 / \tan^2\theta_0$ and $\delta 2\theta / (\tan\theta_0 \sin\theta_0)$ is obtained by fitting, as shown in Fig. 7. The values of d, ($\langle e^2\rangle^{1/2}$), and ρ are calculated on the basis of the slope of the fitted straight line and the y-axis intercept; the results are shown in Table 2.

Fig. 7 shows that the y-intercept of the fitted straight line is a negative value; however, the material's dislocation density cannot be negative. The dislocation density was therefore regarded as 0, indicating that the dislocation density after the pre-recovery heat treatment was negligible. Comparing the dislocation density of the alloy under different states reveals that the pre-recovery heat treatment substantially reduced the alloy's dislocation density.

3.3. Hardness and conductivity

The hardness and electrical conductivity in the Z direction of the rolled Al–12.18Zn–3.31Mg–1.43Cu–0.20Zr–0.04Sr alloy under different aging processes are listed in Table 3. According to the data in Table 3, the aging process strongly affects the hardness and electrical conductivity of the material. The hardness of the material aged under the T7X-1

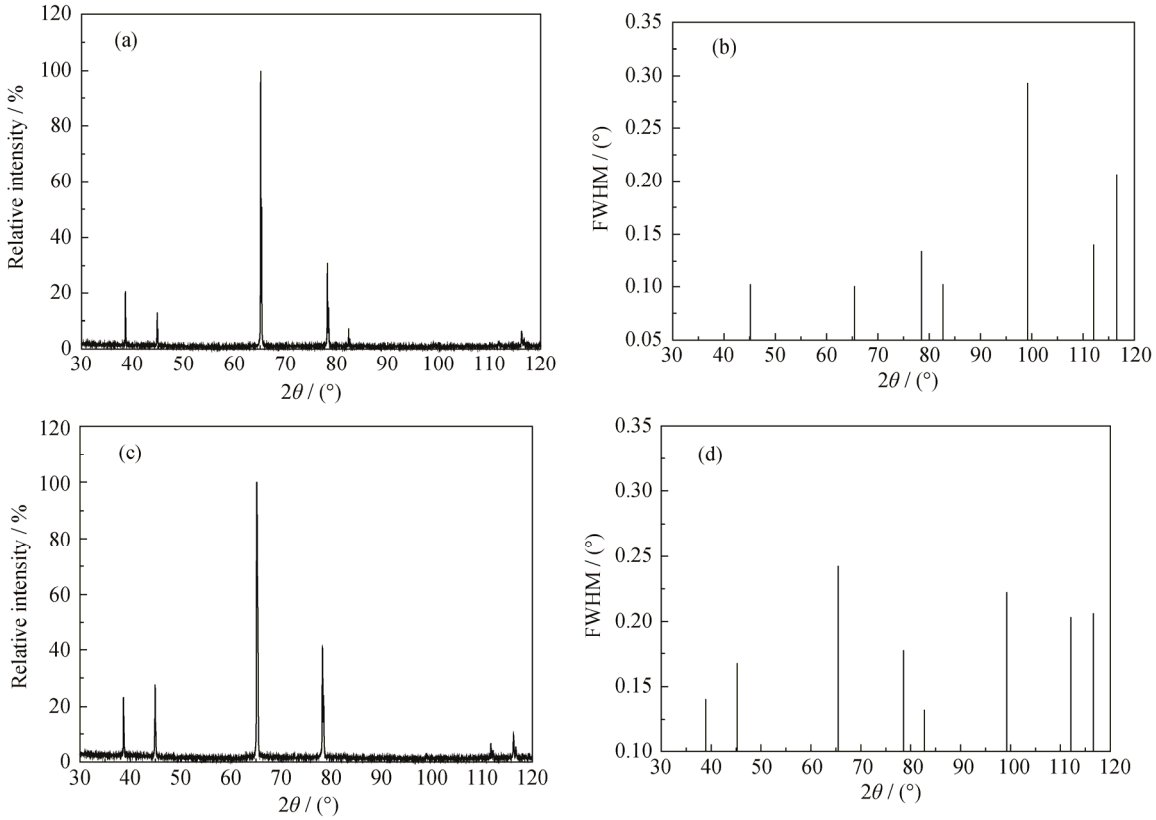

Fig. 6. The XRD patterns (a, c) and FWHMs (b, d) of alloy samples subjected to different heat treatment processes: (a) and (b)—rolling–solution; (c) and (d)—rolling–pre-recovery–solution

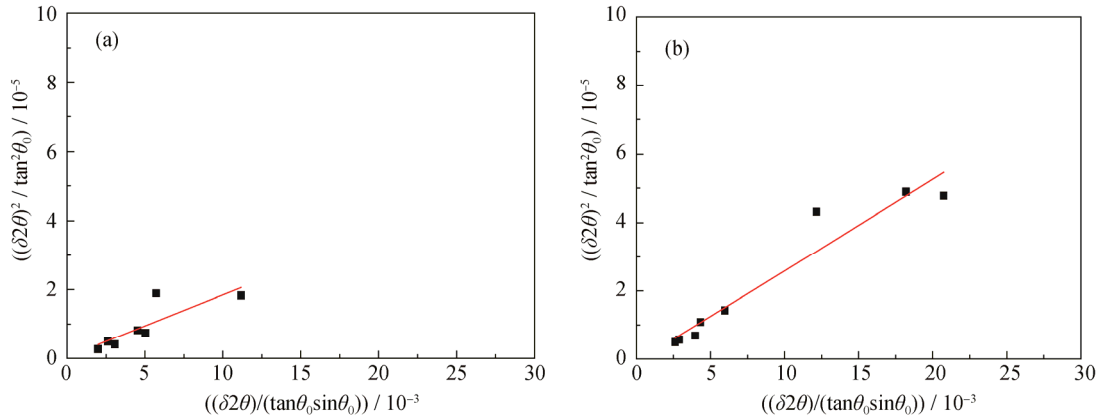

Fig. 7. The fitting relationships between $(\delta 2\theta)^2/\tan^2\theta_0$ and $\delta 2\theta/(\tan\theta_0\sin\theta_0)$: (a) rolling–solution; (b) rolling–pre-recovery–solution.

Table 2. The calculated parameters based on the XRD data

State	d / nm	$\langle e^2\rangle^{1/2}$	ρ / (10^{14} m^{-2})
Rolling–Solution	85.1160	1.290×10^{-4}	0.1835
Rolling–Pre-recovery–Solution	57.7003	0	0

process is obviously lower than that of the materials aged under the T6 and T7X-2 processes; however, the electrical conductivity is substantially greater than that under the other two aging processes. The hardness is highest for the alloy aged under the T7X-2 process, followed by alloys aged under the T6 and T7X-1 processes. Contrary to the change-in-hardness trend, the electrical conductivity is highest for the sample aged under the T7X-1 process, followed by the samples aged under the T7X-2 and T6 processes. The intergranular corrosion resistance of the aluminum alloy has a certain positive correlation with its electrical conductivity; we therefore speculated that the alloy's intergranular corrosion resistance would be highest for the sample aged under the T7X-1 process [14–15]. Under the same aging process, the hardness and electrical conductivity of the material did not substantially change, which indicates

that the pre-recovery heat treatment had little effect on the hardness and electrical conductivity of the material.

The conductivity of a metallic material is usually related to its temperature and to its various internal defects such as impurities, dislocations, and lattice distortion [16]. For this aluminum alloy, the electrical conductivity of the sample aged under the T7X-1 process is the highest; this phenomenon is attributed to the high aging process temperature. After the T7X-1 aging process treatment, the precipitates in the alloy were mainly noncoherent precipitation phases of the matrix. The decrease of the coherent precipitation phase of the original matrix can lead to the disappearance of the stress field around the original coherent precipitates. In addition, the high aging process temperature can also increase the size of the precipitated phase in the alloy and decrease the solid solubility of the matrix and the degree of lattice distortion. The decrease of the coherent precipitated phase and solid solubility and the increase in precipitated phase size will collectively increase the mobility of the conductive electrons in the alloy, thereby leading to an increase of electrical conductivity.

Table 3. Hardness and conductivity of this alloy

Treatment		Hardness, HV	Conductivity / ($S \cdot m^{-1}$)
Rolling–solution	T6	245.1	1.57006
	T7X-1	239.7	1.80961
	T7X-2	249.2	1.60022
Rolling–Pre-recovery–solution	T6	242.3	1.48016
	T7X-1	231.6	1.82991
	T7X-2	251.6	1.60133

3.4. Tensile properties

Table 4 shows the tensile properties of the alloy under different processes in the *X* and *Y* directions. The alloy has high tensile strength under all three aging processes, and the strength reaches 700 MPa; however, the elongation is low and the plasticity is poor. In addition, the tensile properties of the material in the *X* and *Y* directions differ only slightly, which indicates that the tensile properties of the material have a certain degree of isotropy; the pre-recovery heat treatment does not change this property. The tensile strength of the alloy varies greatly under different aging conditions. The tensile strength of the material aged under the T7X-2 process is the highest, followed by those of the materials aged under the T6 and T7X-1 processes; this rule is consistent with the hardness under different aging conditions. Under the same aging process, the tensile strength in the *X* and *Y* direction of the alloy after the pre-recovery treatment was greatly improved compared with that of the alloy in the rolling–solid solution state. The *X*-direction tensile strength of the material subjected to the T7X-2 aging process increased from 785.0 MPa to 809.2 MPa, and the maximum tensile strength reached 800 MPa. Thus, the pre-recovery heat treatment has a substantial strengthening effect on the aluminum alloy and can obviously increase its tensile strength.

Table 4. The tensile properties of the alloy under different processes

State and direction		Tensile strength / MPa	Elongation / %
Rolling–solution	Y-T6	760.0	4.5
	X-T6	739.0	4.0
	X-(T7X-1)	717.1	5.0
	X-(T7X-2)	785.0	4.8
Rolling–pre-recovery–solution	Y-T6	793.4	2.5
	X-T6	767.6	2.5
	X-(T7X-1)	752.1	3.8
	X-(T7X-2)	809.2	5.8

Figs. 8 and 9 show the tensile fracture morphologies in the *X* and *Y* directions of the alloy under three different aging treatments. The tensile fracture morphologies indicate that the fracture forms of the alloy under different aging processes are brittle fractures, which are mainly intergranular fractures with partial plastic fracture characteristics in certain regions. Under the same aging process, the pre-recovery treatment has little effect on the fracture behavior of the material, consistent with the law of the elongation data. Hence, the effect of pre-recovery on the plasticity of this material is negligible.

3.5. Intergranular and exfoliation corrosion resistance

Fig. 10 shows the intergranular corrosion morphologies and the intergranular corrosion depth of the aluminum alloy under different heat treatment processes. The intergranular corrosion rank and exfoliation corrosion rank are listed in Table 5. The intergranular corrosion of aluminum alloy usually germinates from the grain boundaries and then gradually extends to the interior of the alloy along the grain boundaries, resulting in a reduction of the bonding force between the grains and a decrease of the alloy's strength, which can seriously weaken the overall performance of the material [17]. The results in Fig. 10 and Table 5 show that the aging process strongly affects the alloy's resistance to intergranular corrosion. For alloy samples under different heat treatment conditions, the intergranular corrosion resistance of the sample aged under the T7X-1 process is best, which is also consistent with the law of conductivity. After rolling–pre-recovery–solution heat treatment, the depth of

intergranular corrosion of the alloy under the T7X-1 aging process is only 60.81 μm, which is substantially lower than that of 131.32 μm for the alloy under the T6 aging process and that of 126.03 μm for the alloy under the T7X-2 aging process. Under the same aging process, the intergranular corrosion resistance of this material after pre-recovery heat treatment did not obviously change. After rolling–solution or rolling–pre-recovery–solution treatment, the depth of intergranular corrosion is similar and the rank of intergranular corrosion is the same, indicating that the pre-recovery heat treatment has no obvious effect on the alloy's intergranular corrosion resistance.

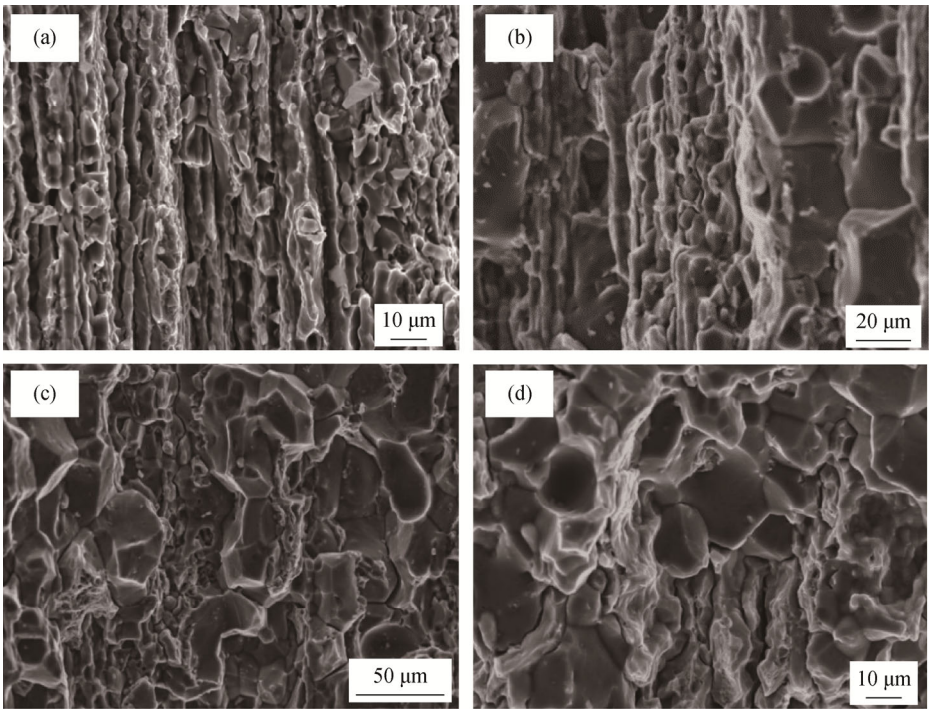

Fig. 8. The tensile fracture morphologies of the alloy after rolling–solution treatment: (a) T6-Y; (b) T6-X; (c) (T7X-1)-X; (d) (T7X-2)-X.

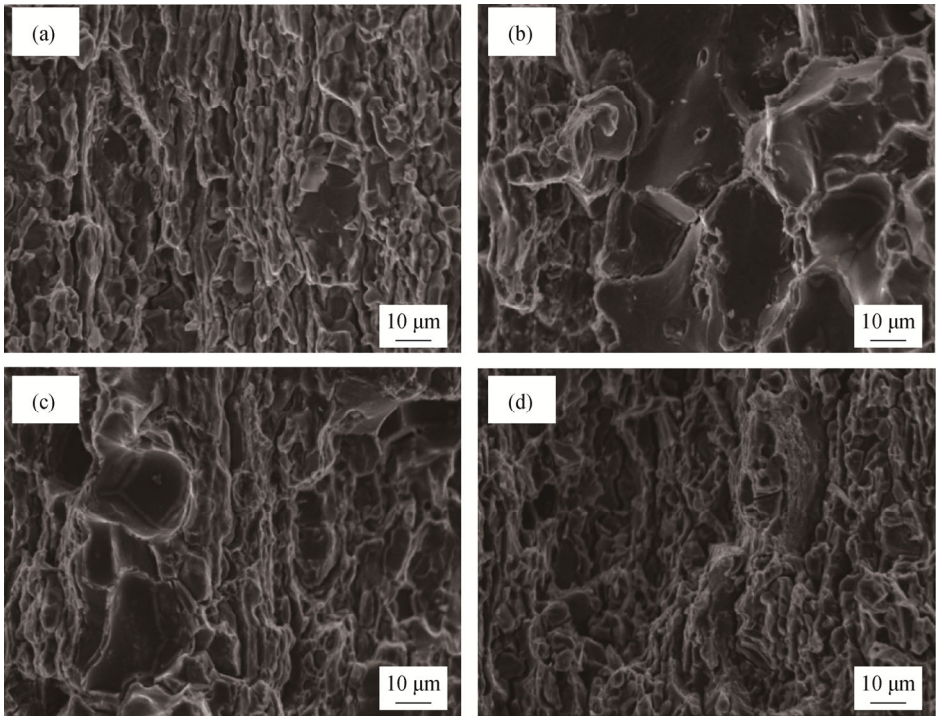

Fig. 9. The tensile fracture morphologies of the alloy after rolling–pre-recovery–solution treatment: (a) T6-Y; (b) T6-X; (c) (T7X-1)-X; (d) (T7X-2)-X.

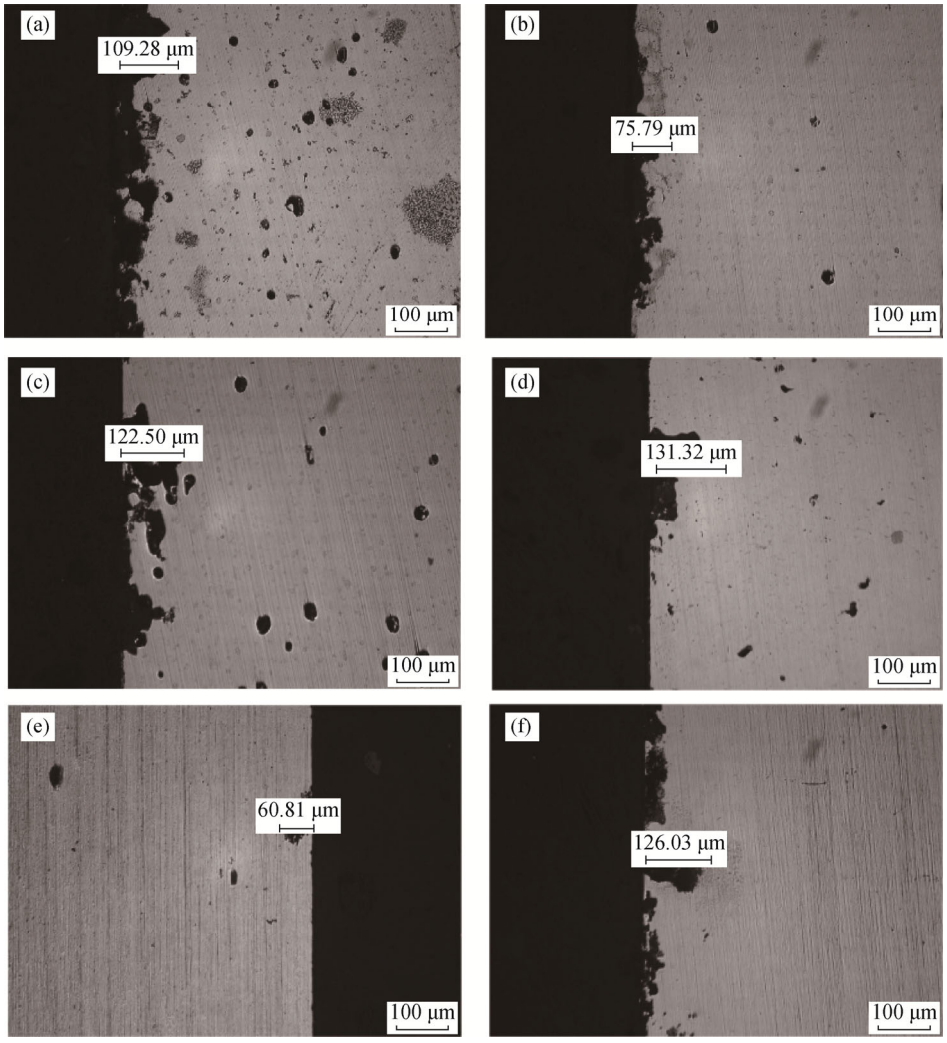

Fig. 10. Intergranular corrosion morphologies under different conditions. Rolling–solution-aging: (a) T6; (b) T7X-1; (c) T7X-2. Rolling–pre-recovery–solution-aging: (d) T6; (e) T7X-1; (f) T7X-2.

There are two main reasons for the formation of intergranular corrosion: First, a nonuniform internal composition and differences in the microstructure of the material can diminish the material's corrosion resistance and easily result in intergranular corrosion. Second, the dissolution of the grain-boundary precipitates can form a closed corrosive environment, resulting in the expansion of corrosion inside the material along the grain boundaries and the formation of continuous corrosion. For this alloy, the reason the material aged under the T7X-1 process exhibits the best intergranular corrosion resistance may be that the higher aging temperature consumes more deformation energy stored in the material, reduces the grain-boundary energy and promotes dissolution of the undissolved second phase, thus interrupting the intergranular corrosion channel and improving the alloy's resistance to intergranular corrosion.

Fig. 11 shows the exfoliation corrosion morphologies of the Al–12.18Zn–3.31Mg–1.43Cu–0.20Zr–0.04Sr aluminum alloy under different heat treatment processes. The morphologies indicate that all of the samples underwent exfoliation corrosion with corrosion ranks between EA and EB. Comparing the exfoliation corrosion under three aging processes reveals that the exfoliation corrosion resistance under T7X-2 aging process is the worst, with an exfoliation corrosion rank of EB. The exfoliation corrosion resistances of the alloy under T6 and T7X-1 aging processes show little difference, and the exfoliation corrosion ranks are all EA. Under the same aging process, the morphologies of exfoliation corrosion with rolling–pre-recovery–solution treatment or rolling–solution treatment differ only slightly. This phenomenon illustrates that the pre-recovery heat treatment has little effect on the exfoliation corrosion resistance of this aluminum alloy.

Exfoliation corrosion has been widely speculated to develop from intergranular corrosion and to be related to the grain-boundary morphology and precipitates of the material;

it tends to occur in alloys with a large length-to-diameter ratio [18–19]. In this experiment, the pre-recovery heat treatment does not dramatically alter the morphology of the alloy and it also has little effect on the grain size of the material. Therefore, the effect of the pre-recovery heat treatment on the exfoliation corrosion resistance of this alloy is negligible.

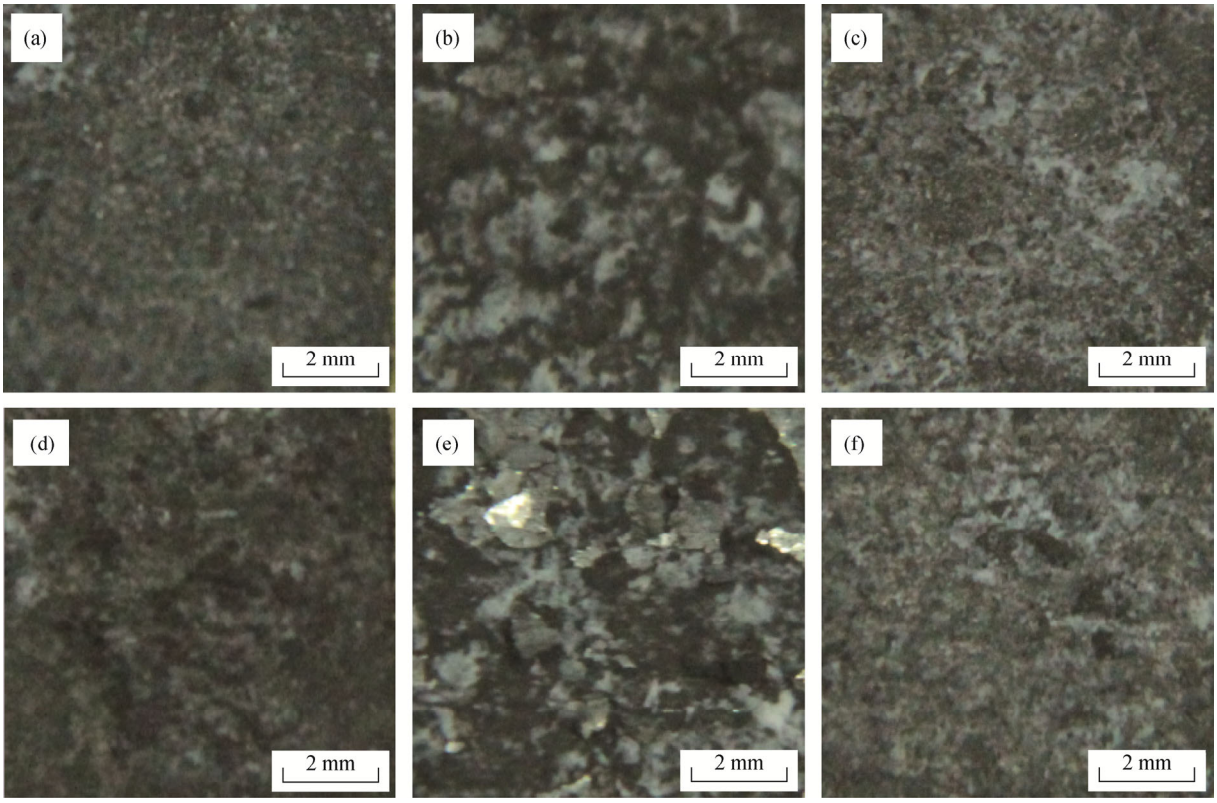

Fig. 11. Exfoliation corrosion morphologies under different conditions. Rolling–solution-aging: (a) T6; (b) T7X-1; (c) T7X-2. Rolling–pre-recovery–solution-aging: (d) T6; (e) T7X-1; (f) T7X-2.

Table 5. The intergranular corrosion depth, rank, and exfoliation corrosion rank of the alloy under different conditions

Treatment		Intergranular corrosion depth / μm	Intergranular corrosion rank	Exfoliation corrosion rank
Rolling–solution	T6	109.28	Fourth	EA
	T7X-1	75.79	Third	EA
	T7X-2	122.50	Fourth	EB
Rolling–pre-recovery–solution	T6	131.32	Fourth	EA
	T7X-1	60.81	Third	EA
	T7X-2	126.03	Fourth	EB

4. Conclusions

The Al–12.18Zn–3.31Mg–1.43Cu–0.20Zr–0.04Sr aluminum alloy used in this experiment, after hot extrusion and rolling processing, contained extensive deformation energy. In the subsequent solution treatment processing, the alloy was prone to recrystallization because of the high solution temperature, which could weaken the alloy's strength and diminish its usability. However, the introduction of a pre-recovery heat treatment substantially improved the material's performance.

(1) The pre-recovery heat treatment has little effect on the crystal orientation of Al–12.18Zn–3.31Mg–1.43Cu–0.20Zr–0.04Sr aluminum alloy, but it promotes the dissolution of undissolved second phase, consumes deformation energy, inhibits recrystallization, and substantially reduces the dislocation density.

(2) The pre-recovery heat treatment has little effect on the hardness, electrical conductivity, and elongation of this aluminum alloy; however, it can obviously increase the tensile

strength (the maximum tensile strength increased from 785.0 MPa to 809.2 MPa). Moreover, the tensile properties of this alloy exhibit a certain degree of isotropy and the pre-recovery heat treatment does not change this property.

(3) The Al–12.18Zn–3.31Mg–1.43Cu–0.20Zr–0.04Sr aluminum alloy has good corrosion resistance; the effect of the pre-recovery heat treatment on the alloy's resistance to intergranular and exfoliation corrosion is negligible.

Acknowledgements

This work was financially supported by the Jiangsu Provincial Industrial Science and Technology Support Program (No. BE2008118) and the Basic Research on Isotropic Ultra-high Strength Aluminum Matrix Composite (No. 6140922010201).

References

[1] S.D. Liu, Q. Li, H.Q. Lin, L. Sun, T. Long, L.Y. Ye, and Y.L. Deng, Effect of quench-induced precipitation on microstructure and mechanical properties of 7085 aluminum alloy, *Mater. Des*., 132(2017), p. 119.

[2] D.F. Li, D.Z. Zhang, S.D. Liu, Z.J. Shan, X.M. Zhang, Q. Wang, and S.Q. Han, Dynamic recrystallization behavior of 7085 aluminum alloy during hot deformation, *Trans. Nonferrous Met. Soc. China*, 26(2016), No. 6, p. 1491.

[3] Y.L. Zheng, C.B. Li, S.D. Liu, Y.L. Deng, and X.M. Zhang, Effect of homogenization time on quench sensitivity of 7085 aluminum alloy, *Trans. Nonferrous Met. Soc. China*, 24(2014), No. 7, p. 2275.

[4] D. Singh, P.N. Rao, and R. Jayaganthan, Microstructures and impact toughness behavior of Al 5083 alloy processed by cryorolling and afterwards annealing, *Int. J. Miner. Metall. Mater*., 20(2013), No. 8, p. 759.

[5] R.G. Guan, X. Wang, Z.Y. Zhao, W.W. Wang, F.R. Cao, and C.M. Liu, Microstructure and properties of A2017 alloy strips processed by a novel process by combining semisolid rolling, deep rolling, and heat treatment, *Int. J. Miner. Metall. Mater*., 20(2013), No. 8, p. 770.

[6] X.P. Li, C.Y. Liu, M.Z. Ma, and R.P. Liu, Microstructures and mechanical properties of AA6061-SiC composites prepared through spark plasma sintering and hot rolling, *Mater. Sci. Eng. A*, 650(2016), p. 139.

[7] X.J. Xu, Y.K. Zhang, P.A. Deng, Y. Wu, Z.Q. Zhang and Y.D. Lu, Effect of pre-recovery-annealing treatment on microstructure and properties of extruded 7085 aluminum alloy, *Trans. Mater. Heat Treat.*, 35(2014), No. 8, p. 36.

[8] L.S. Sun, X.J. Xu, W. Jiang, and Y.X. Fan, Effect of pre-recovery treatment on microstructure and properties of extruded Al–13.0Zn–3.16Mg–2.8Cu–0.2Zr–0.07Sr aluminum alloy, *Trans. Mater. Heat Treat.*, 36(2015), No. 12, p. 61.

[9] A. Dhal, S.K. Panigrahi, and M.S. Shunmugam, Insight into the microstructural evolution during cryo-severe plastic deformation and post-deformation annealing of aluminum and its alloys, *J. Alloys Compd*., 726(2017), p. 1205.

[10] Z.Y. Guo, G. Zhao, and X.G. Chen, Effects of homogenization treatment on recrystallization behavior of 7150 aluminum sheet during post-rolling annealing, *Mater. Charact*., 114(2016), p. 79.

[11] Q.Y. Yang, Z.H. Deng, Z.Q. Zhang, Q. Liu, Z.H. Jia, and G.J. Huang, Effects of strain rate on flow stress behavior and dynamic recrystallization mechanism of Al–Zn–Mg–Cu aluminum alloy during hot deformation, *Mater. Sci. Eng. A*, 662(2016), p. 204.

[12] X.J. Xu, C.S. W, Y.F. Guo, Q. Ding, J. Huang, J.X. Zhu, and F. Yang, Effect of solid solution-cold deformation-prerecovery on microstructure and properties of Al–13.01Zn–3.16Mg–2.8Cu–0.204Zr–0.0757Sr aluminum alloy, *Trans. Mater. Heat Treat.*, 38(2017), No. 1, p. 37.

[13] X.L. Zhang, X.J. Xu, Z.Y. Ling, and W. Jiang, Microstructure and mechanical properties of an extruded Al-alloy Al–10.78Zn–2.78Mg–2.59Cu–0.22Zr–0.047Sr, *Chin. J. Mater. Res*., 29(2015), No. 10, p. 729.

[14] M. Lipińska, P. Bazarnik, and M. Lewandowska, The influence of severe plastic deformation processes on electrical conductivity of commercially pure aluminium and 5483 aluminium alloy, *Arch. Civ. Mech. Eng*., 16(2016), No. 4, p. 717.

[15] F.D. Zhang, H. Liu, C. Suebka, Y.X. Liu, Z. Liu, W. Guo, Y.M. Cheng, S.L. Zhang, and L. Li, Corrosion behaviour of laser-cleaned AA7024 aluminium alloy, *Appl. Surf. Sci.*, 435(2018), p. 452.

[16] X.L. Cui, Y.Y. Wu, X.F. Liu, Q.R. Zhao, and G.J. Zhang, Effects of grain refinement and boron treatment on electrical conductivity and mechanical properties of AA1070 aluminum, *Mater. Des*., 86(2015) , p. 397.

[17] Z.X. Wang, P. Chen, H. Li, B.J. Fang, R.G. Song, and Z.Q. Zheng, The intergranular corrosion susceptibility of 2024 Al alloy during re-aging after solution treating and cold-rolling, *Corros. Sci.*, 114(2017), p. 156.

[18] F.X. Song, X.M. Zhang, S.D. Liu, Q. Tan, and D.F. Li, Exfoliation corrosion behavior of 7050-T6aluminum alloy treated with various quench transfer time, *Trans. Nonferrous Met. Soc. China*, 24(2014), No. 7, p. 2258.

[19] A.S. Verma, Sumankant, N.M. Suri, and Yashpal, Corrosion behavior of aluminum base particulate metal matrix composites: A review, *Mater. Today. Proc*., 2(2015), No. 4-5, p. 2840